Article

Geological Conditions of Shale Gas Accumulation in Coal Measures

Fengchu Liao [1], Keying Wang [1,2,3,*], Jian Zhan [1,2], Zhiwei Liu [1,2], Jiang Du [1,2], Shuhua Gong [1,2], Ningbo Cai [1,2,3], Jianglun Bai [4] and Junjian Zhang [4]

[1]   Geophysical and Geochemical Survey Institute of Hunan Province, Changsha 410014, China; liaofc123456@163.com (F.L.); zhanjian0822@163.com (J.Z.); liuzhiwei6657@163.com (Z.L.); dujiangcumt@163.com (J.D.); shgong10@126.com (S.G.); cainb666@163.com (N.C.)
[2]   Hunan Geological New Energy Exploration and Development Engineering Technology Research Center, Changsha 410014, China
[3]   Institute of Advanced Study, China University of Geosciences (Wuhan), Wuhan 430070, China
[4]   College of Earth Sciences & Engineering, Shandong University of Science and Technology, Qingdao 266590, China; 18803661662@163.com (J.B.); junjianzhangcumt@126.com (J.Z.)
[*]   Correspondence: wangjx3327225@163.com

Abstract: The shale of different potential layers is studied by using rock pyrolysis analysis, total organic carbon determination (TOC), kerogen microscopic component identification, mineral X-ray diffraction, scanning electron microscopy, and low-temperature nitrogen adsorption experiments. The results are as follows: (1) Shishui Formation of the Lower Carboniferous and Longtan Formation of the Upper Permian are the two most important shale gas reservoirs in the Chenlei Depression. The sedimentary environment of the target shale is a marine land interaction facies coastal bay lagoon swamp sedimentary system. Two sedimentary facies of tidal flat facies, subtidal zone, and lagoon swamp facies are developed. (2) The organic matter types of shale are Type III and II_2, with TOC content greater than 1%. The maturity of shale samples is relatively higher ($R_{o,max}$ is above 2%), which means they have entered the stage of large-scale gas generation. The overall brittle mineral content of the target shale sample is relatively higher (above 40%), which is conducive to artificial fracturing and fracture formation in the later stage, while an appropriate amount of clay minerals (generally stable at 40%) is conducive to gas adsorption. (3) The overall pore structure of the water measurement group and Longtan group is good, with a higher specific surface area and total pore volume (average specific surface area is 12.21 and 8.36 m^2/g, respectively), which is conducive to the occurrence of shale gas and has good adsorption and storage potential. The gas content of the water measurement group and the Longtan Formation varies from 0.42 to 5 cm^3/g, with an average of 2.1 cm^3/g. It indicates that the water measurement group and the Longtan Formation shale gas in the study area have good resource potential.

Keywords: shale gas; physical property; gas content; pore structure; resource potential

1. Introduction

With the development of oil and gas exploration in China, shale gas as an important strategic alternative energy has received more and more attention [1]. The geological conditions for shale gas accumulation are the theoretical basis for achieving breakthroughs in shale gas exploration [2–6]. Related literature has systematically evaluated the geological conditions for shale gas accumulation in different regions from the perspectives of sedimentary environment, shale thickness, organic matter content, mineral composition, and gas content [7–9]. Based on this, the main controlling factors affecting the enrichment of shale gas reservoirs have also been determined [10,11].

Breakthroughs have been made in marine shale gas exploration in southern China in the upper Yangtze region [12–14]. However, multiple rounds of exploration have been

carried out in the middle and lower Yangzi regions over the years, but there have been no large-scale gas fields [15–18]. As a key area of marine shale gas in the middle and lower Yangzi regions of China, shale gas exploration in the Chenlei Sag, southeast of Hunan Province, is still lower. In recent years, related literature has shown that the possibility of shale gas accumulation in the Chenlei Depression in terms of hydrocarbon source conditions, reservoir characteristics, and structural evolution [12,19]. Cao et al. studied the hydrocarbon source and porosity of shale in the lower carboniferous Yanguanjie Formation [20]. Luo et al. and Cao et al. studied the mud shale of the Longtan Formation and concluded that the mud shale of the Longtan Formation has good reservoir properties [2]. Yin et al. studied the relationship between geological structural characteristics and coal seams [21]. Shi et al. discussed the tectonic evolution of the area and its relationship with oil and gas accumulation [22].

Above all, some research has been done on the geological conditions for shale gas reservoir formation. However, there are still several issues that need to be addressed. Firstly, the method for determining the main controlling factors of shale gas reservoir formation and geological conditions needs to be explored. In addition, further research is needed on the geological conditions for shale gas accumulation in this study area. Finally, the target shale rock layers in the study area are not yet clear.

In this paper, geological conditions for the formation of shale gas reservoirs in the coal bearing strata of Chenlei Depression, Hunan Province, have been studied. The main target layer for shale gas occurrence has been determined through shale thickness and sedimentary facies analysis. Rock pyrolysis analysis, total organic carbon determination (TOC), kerogen microscopic component identification, mineral X-ray diffraction, scanning electron microscopy, and low-temperature nitrogen adsorption experiments are used to study the geological conditions of shale gas. On this basis, the sedimentary environment/thickness/physical properties (porosity and permeability)/gas content of shale reservoirs in different formations are studied, the basic geological conditions of shale gas in the target rock layers are determined, and favorable areas for shale gas development are determined.

2. Geological Setting and Experimental Methods

2.1. Geological Setting

The study area is located in the southeastern margin of the southeastern Hunan Depression. The Chenlei Depression is a secondary tectonic unit of the southeastern Hunan Depression. It is bounded by a fault zone to the northwest and adjacent to the Hengshan uplift zone, separated by a fault zone to the north and east from the Cathaysia fold belt, and gradually transitioning to the Ningjiang bulge in the southwest in the form of a slope zone (Figure 1). The southeast Hunan Depression is located in the southeast of Hunan Province, geotectonically situated in the south china plate and Yangzi plate junction, as a whole is part of the south china fold system [23]. The study area has experienced the superimposed influence of multi-stage tectonic cycles, and the tectonic lines are crisscrossing and extremely complex, and the folds and faults are developed. The southeastern part of the Chenlei Depression in the Linwu area is a Caledonian fold belt, with structural lines mainly trending NNE~SSW and dipping southeast. It is a tight anticline with a reverse fault parallel to the fold axis, accompanied by the intrusion of granodiorite and diorite. In the central and western parts of the depression, there is an Indonesian fold belt that runs through the entire area from north to south [24–27].

The study area is well developed and distributed from the Proterozoic to Cenozoic (Figure 1). The basement is built of flysch in the Proterozoic and Lower Paleozoic. The lithology is mainly slate and carbonate. From the Devonian Period of the Late Paleozoic Era to the Early Triassic Period of the Mesozoic Era, the deposits were platform-type littoral-shallow marine strata, the lithology was carbonate rock and coal-bearing clastic rock, and a variety of shale strata were developed. The study area entered the continental sedimentary period from the Middle Triassic. Only the Middle Jurassic strata remain today.

The lithology is interbedded sandstone and mudstone. After the Late Mesozoic Cretaceous period, multiple phases of fault depression occurred due to extensional movements caused by mantle uplift, resulting in the deposition of a set of red clastic rocks. The fourth department is the residual slope, and the accumulation layer is not developed [17]. Dark mudstones and shales developed in the Middle to Upper Devonian, Lower Carboniferous, and Upper Permian of the Late Paleozoic within cratonic platform-type coastal shallow marine and coal-bearing clastic rock formations of marine–terrestrial transitional facies.
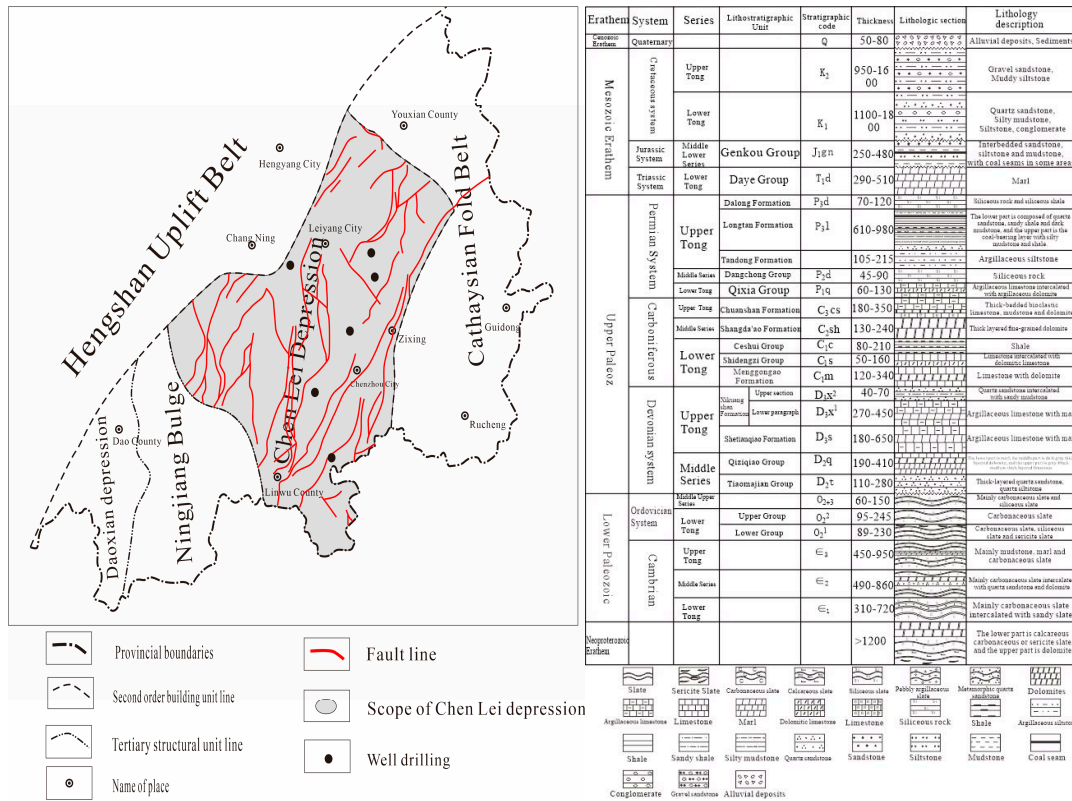
Erathem	System	Series	Lithostratigraphic Unit	Stratigraphic code	Thickness	Lithologic section	Lithology description
Cenozoic Erathem	Quaternary			Q	50–80		Alluvial deposits, Sediments
Mesozoic Erathem	Cretaceous system	Upper Tong		K_2	950–1600		Gravel sandstone, Muddy sandstone
	Cretaceous system	Lower Tong		K_1	1100–1800		Quartz sandstone, Silty mudstone, Siltstone, conglomerate
	Jurassic System	Middle Lower Series	Genkou Group	J_1gn	250–480		Interbedded sandstone, siltstone and mudstone, with coal seams in some areas
	Triassic System	Lower Tong	Daye Group	T_1d	290–510		Marl
Upper Paleoz	Permian System	Upper Tong	Dalong Formation	P_3d	70–120		Siliceous rock and siliceous shale
		Upper Tong	Longtan Formation	P_3l	610–980		The lower part is composed of quartz sandstone, sandy shale and dark mudstone, and the upper part is the coal-bearing layer with silty mudstone and shale.
		Upper Tong	Tandong Formation		105–215		Argillaceous siltstone
		Middle Series	Dangchong Group	P_2d	45–90		Siliceous rock
		Lower Tong	Qixia Group	P_1q	60–130		Argillaceous limestone intercalated with argillaceous dolomite
	Carboniferous	Upper Tong	Chuanshan Formation	C_3cs	180–350		Thick-bedded bioclastic limestone, mudstone and dolomite
		Middle Series	Shangda'ao Formation	C_2sh	130–240		Thick layered fine-grained limestone
		Lower Tong	Ceshui Group	C_1c	80–210		Shale
		Lower Tong	Shidengzi Group	C_1s	50–160		Limestone intercalated with dolomitic limestone
		Lower Tong	Menggongao Formation	C_1m	120–340		Limestone with dolomite
	Devonian system	Upper Tong	Xikuang shan Formation Upper section	D_3x^2	40–70		Quartz sandstone intercalated with sandy mudstone
		Upper Tong	Xikuang shan Formation Lower paragraph	D_3x^1	270–450		Argillaceous limestone with marl
		Upper Tong	Shetianqiao Formation	D_3s	180–650		Argillaceous limestone with marl
		Middle Series	Qiziqiao Group	D_2q	190–410		Thick-layered quartz sandstone, quartz siltstone
		Middle Series	Tiaomajian Group	D_2t	110–280		Mainly carbonaceous slate and siliceous slate
Lower Paleozoic	Ordovician System	Middle Upper Series		O_{2+3}	60–150		Mainly carbonaceous slate and siliceous slate
		Lower Tong	Upper Group	O_1^2	95–245		Carbonaceous slate
		Lower Tong	Lower Group	O_1^1	89–230		Carbonaceous slate, siliceous slate and sericite slate
	Cambrian	Upper Tong		$\in_3$	450–950		Mainly mudstone, marl and carbonaceous slate
		Middle Series		$\in_2$	490–860		Mainly carbonaceous slate intercalated with quartz sandstone and dolomite
		Lower Tong		$\in_1$	310–720		Mainly carbonaceous slate intercalated with sandy slate
Neoproterozoic Erathem					>1200		The lower part is calcareous carbonaceous or sericite slate, and the upper part is dolomite

Map legend: Provincial boundaries; Second order building unit line; Tertiary structural unit line; Name of place; Fault line; Scope of Chen Lei depression; Well drilling.

Lithology symbols: Slate; Sericite Slate; Carbonaceous slate; Calcareous slate; Siliceous slate; Pebbly argillaceous slate; Metamorphic quartz sandstone; Dolomites; Argillaceous limestone; Limestone; Marl; Dolomitic limestone; Limestone; Siliceous rock; Shale; Argillaceous siltstone; Shale; Sandy shale; Silty mudstone; Quartz sandstone; Sandstone; Siltstone; Mudstone; Coal seam; Conglomerate; Gravel sandstone; Alluvial deposits.

Figure 1. Study area location and stratum formation.

2.2. Experimental Methods

High-pressure mercury intrusion test (HPMI). The most commonly used method to analyze the seepage pore structure of coal reservoirs is the HPMI method. It determines essential information such as porosity, pore structure, pore connectivity, and the pore compression coefficient of coal. This test overcomes capillary forces by gradually increasing the pressure of the mercury injection. The maximum mercury inlet pressure for this test is 14.7 MPa, covering a test pore size range of 3~10,000 nm.

Low-temperature carbon dioxide/nitrogen adsorption test (LTCO$_2$/N$_2$ GA). In this test, 20 g of each sample is selected and ground to a particle size of 40–60 mesh. LTCO$_2$/N$_2$ GA is the prevailing method for analyzing the adsorption pore structure of coal reservoirs, providing insights into parameters such as porosity, pore structure, and pore connectivity. The TriStar III 3020 surface area and pore size distribution analyzer was used to detect the surface morphology of adsorption pores at 77 K. The PV and SSA of meso-pores (2~100 nm) are determined using the Barrett–Joyner–Halenda (BJH) model, whereas the PV and SSA of micro-pores (<2 nm) are determined using the density function theory (DFT) model.

3. Results and Discussion

3.1. Sedimentary and Distribution of Shale

From the Late Paleozoic to the Middle Triassic of the Mesozoic, the tectonic environment was stable, and the clastic rock was widely accepted as the main clastic rock.

Several sets of mud shale formations were developed. Among them, the thick dark black carbonaceous shale is developed in the Lower Cambrian Formation of the Carboniferous and upper Longtan Formation of the Permian, and the target shale is the most important potential source of shale gas in the Chenlei Depression.

The sedimentary environment of the Lower Carboniferous Water (LCW) Formation is the sea–land interlocking marina bay lagoon swamp sedimentary system, which develops two sedimentary facies: tidal flat facies subtidal zone and lagoon swamp facies. The subtidal zone of the tidal flat facies is composed of gray siltstone, silty mudstone, and gray black mud shale; it could also contain thin coal seams, which developed in the eastern part of the study area (Figures 2a and 3a). The lagoon swamp facies are composed of fine sandstone, siltstone, sandy mudstone, and thick coal seams interbedded with gray-black to black shale. It is developed in the western part (Figures 2b and 3a). The shale of the Ceshui Formation is distributed in most parts of the depression, but the thickness is thinner, with an average thickness of about 30 m, and the thickness is above the maximum in the southern part of the center of the depression (up to nearly 70 m), corresponding to the lagoon swamp facies deposits, which gradually thin to the north until they peak out.
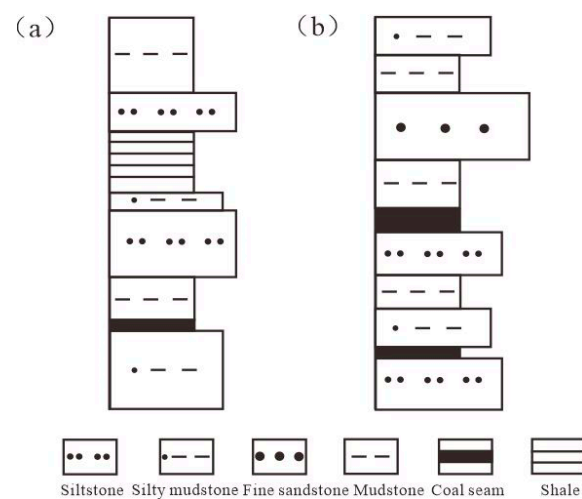
Figure 2. Lithologic combination of different sedimentary facies of Ceshui Formation. ((**a**) Tidal flat facies subtidal zone; (**b**) lagoon swamp facies).
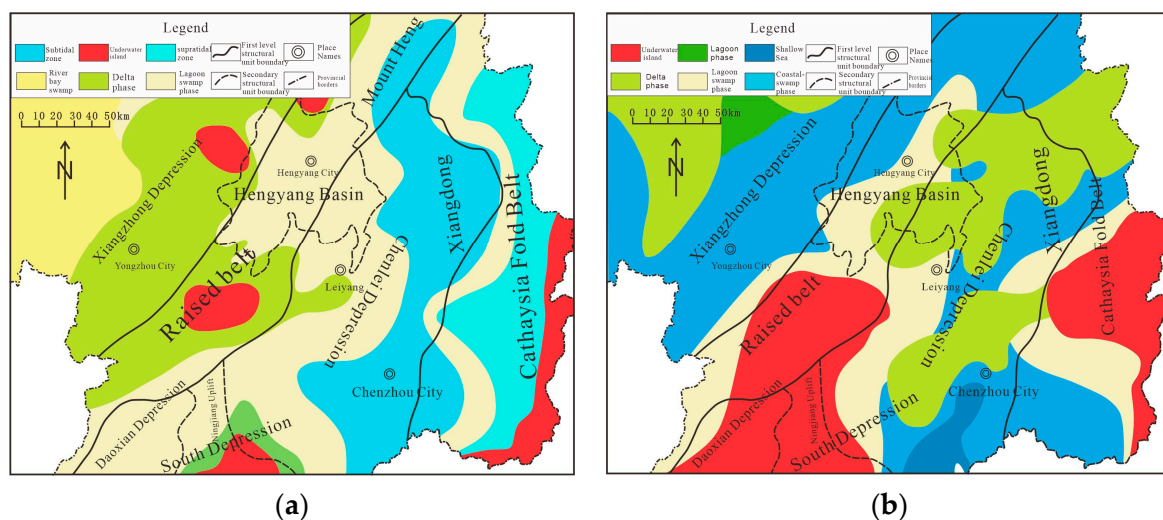
Figure 3. Sedimentary facies plan of Lower Carboniferous Ceshui and Upper Permian Longtan Formation. ((**a**) Ceshui Formation; (**b**) Longtan Formation).

The development types of the Longtan Formation in the Upper Permian include two types: continental sedimentation dominated by delta facies and transitional sedimentation represented by shallow marine, underwater island, lagoon swamp, and coastal swamp facies (Figure 3b). The delta facies are developed in the northwest of the study area, forming a bird-foot-shaped pattern from northeast to southwest. The lithology is composed of thick layers of siltstone and mudstone interbedded with coal seams (Figure 4a). The shallow marine shelf facies are mainly distributed in the southeast. They are primarily affected by the intrusion of seawater from the southeast. The lithology is composed of high calcium content sandy mudstone and mudstone, and the overall thickness of the shale is higher (Figure 4b). The underwater island facies are mainly distributed in the southwest, influenced by ancient landforms, and they are composed of quartz sandstone, medium to fine sandstone, and sand bar facies sedimentation (Figure 4c). The lagoon swamp facies are developed in the central southern part of the Chenlei Depression, and the underwater island facies are northeast. The overall grain size becomes finer, mainly composed of black sandy mudstone, muddy siltstone, and mudstone. The mud shale is thick, with siderite nodules visible (Figure 4d). The coastal swamp facies are distributed in the upper part of the coastline before the ancient continent and are products of the marshification of the coastal plain. They are developed in the eastern and northern parts of the depression, northeast of the lagoon swamp facies, and the lithology is mainly black-gray mud shale and sandy mudstone. The mud shale is thick and is the main environment for mud shale deposition (Figure 4e). The underwater island sand bar is developed from the southwest. The deltaic sediments developed from lagoon-swamp facies to land-facies in the NW direction, indicating a gradual retreat from marine facies to the NE direction of land (Figure 3b).
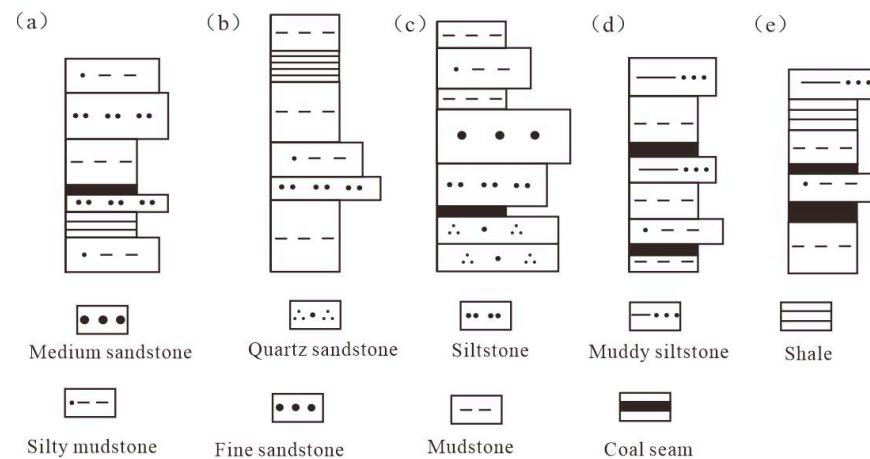
Figure 4. Lithologic combination of different sedimentary facies of Ceshui Formation. ((**a**) Delta facies; (**b**) shallow sea shelf facies; (**c**) underwater island facies; (**d**) lagoon swamp facies; (**e**) coastal swamp facies).

The shale of the Longtan Formation is composed of sandy shale, black shale, carbonaceous shale, etc., and it contains abundant siderite nodules and bands, coexisting with coal seams. The mud shale is almost distributed throughout the entire depression, with a cumulative thickness of large and an average thickness of 100 m(Figure 5a). It is the stratum with the highest thickness of mud shale in the target layer. The thickness of shale in the Longtan Formation matches well with the distribution of sedimentary facies, mainly developed in coal-accumulating environments such as lagoon swamp facies, coastal swamp facies, and delta facies. The maximum thickness of shale in the area between Leiyang and Chenzhou exceeds 200 m (Figure 5b), and it gradually decreases towards the northwest–southeast edges of the depression, with a thickness from 0–50 m.
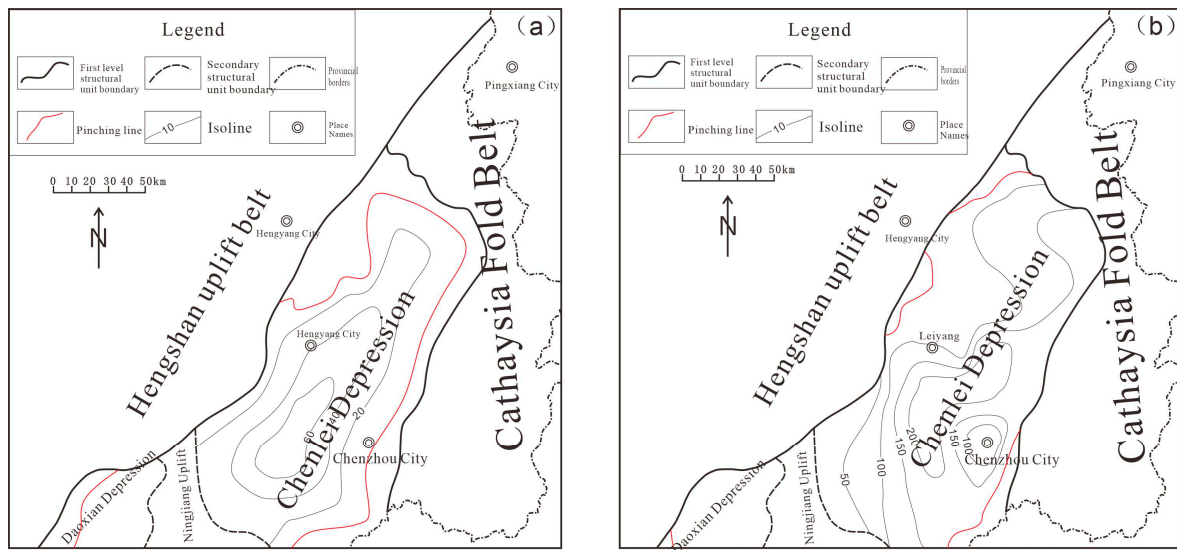
Figure 5. Shale thickness map of geological survey Ceshui and Longtan Formation in Chenlei Sag. ((**a**) Ceshui Formation; (**b**) Longtan Formation).

3.2. Geochemical Characteristics of Shale

3.2.1. Organic Matter Abundance

Based on the total organic carbon (TOC) content of shale in the study area, the TOC values of shale collected from Ceshui and Longtan formations in the Chenlei Depression, southeastern Hunan, are higher (greater than 1%). The TOC of other layers is all below 0.4%, which are source rocks. Therefore, the main hydrocarbon source rock series in the study area belongs to the Ceshui and Longtan formations (Figure 6). Among them, the TOC value of the shale in the Ceshui Formation is the highest, followed by the Longtan Formation. However, they belong to good to excellent high-quality source rocks and have good hydrocarbon generation potential.
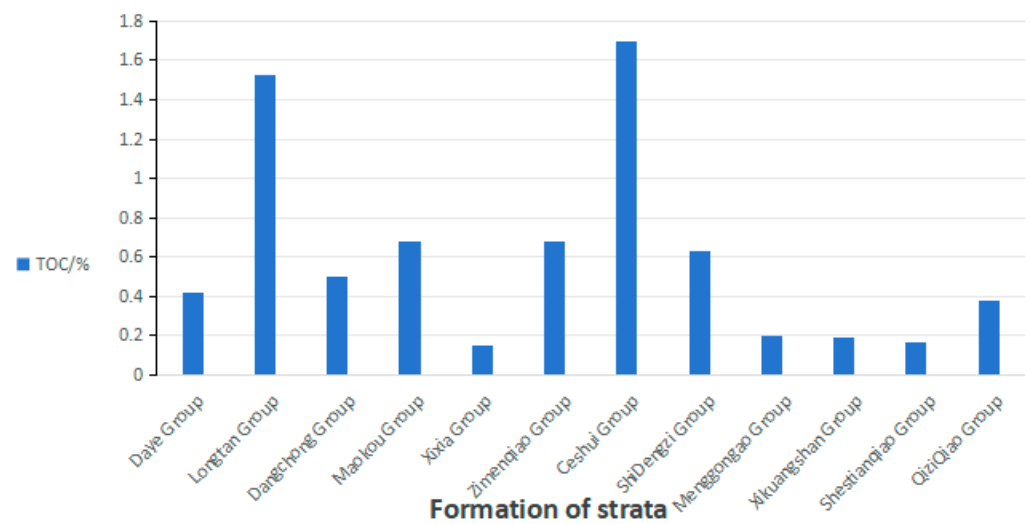
Figure 6. Distribution of organic matter abundance of source rocks in Chenlei Sag.

3.2.2. Organic Matter Type

Based on microscopic identification of components, shale organic matter types in the Chenlei Sag and Longtan Formation are mainly type III and type II_2 (Table 1), and the kerogen type of a small number of samples is type II_1. The Carboniferous-Permian period was a major period of transition from marine to terrestrial phases in geological history. Organisms in the marine and terrestrial transitional phases were unprecedentedly

prosperous. In their chemical composition, lignin, cellulose, and other abundant parent materials were deposited in large quantities, forming a quantitatively superior Type III kerogen, but the contribution of local, deeper organisms evolving into organic matter cannot be ruled out [28,29]. This also shows that the types of organic matter in marine–terrestrial transitional shale are not single. Humic type is the main type, supplemented by mixed type, which provides multiple organic matter for shale hydrocarbon generation.

Table 1. Kerogen macerals of organic-rich shale in Chenlei Sag.

Sampling Layer	Microscopic Component Content/%					Kerogen Type Index (TI)	Kerogen Type
	Sapropel Group	Resin Body	Exinite	Vitrinite	Inert Group		
Ceshui Formation	25	/	56	15	4	37.75	II_2
	21	/	62	14	3	38.5	II_2
Longtan Formation	12	/	66	16	6	27	II_2
	82	/	14	4	/	86	II_1
	64	/	34	2	/	79.5	II_1
	8	/	28	40	24	−32	III
	5	/	20	54	21	−46.5	III
	6	/	30	48	16	−31	III
	8	/	28	50	14	−29.5	III

Rock pyrolysis experiment results show that the Ceshui and Longtan formation shales have TOC values ranging from 1.22 to 10.79 mg/g, with an average of 6.88 mg/g. The hydrogen index values are low, indicating that the organic matter is type III kerogen (Table 2). The reason is that it is the source of humic organic matter. This is related to the excessive maturation of shale (T_{max} is greater than 500 °C) and large-scale occurrences related to hydrocarbon generation. Based on the analysis of kerogen microcomponents and rock pyrolysis, the lithofacies, paleogeography, and geological evolution processes of the region have been studied. The results show that the main source of organic matter in shale is input from terrestrial higher plants, and the main types of organic matter are II_2 and III, which are favorable for the generation of natural gas.

Table 2. Pyrolysis and $R_{o,max}$ data of shale samples from Ceshui and Longtan formations in Chenlei Sag.

Sampling Layer	Sampling No.	Maximum Temperature T_{max} (°C)	Soluble Hydrocarbons S_1 (mg/g)	Pyrolysis Hydrocarbons S_2 (mg/g)	HI (mg/g TOC)	$R_{o,max}$ (%)	Maturity Assessment
Ceshui Formation	CLZH-06	584	0.03	0.84	9.23	2.91	Overmature
	DCLC-03	587	0.04	0.35	9.54	2.99	Overmature
	XJZ-04	585	0.03	0.05	4.39	2.95	Overmature
	ZK3206-87	587	0.03	0.11	4.33	2.37	Overmature
	XDY-74	540	0.04	0.12	15.38	3.51	Overmature
	KJC-68	539	0.05	0.03	1.92	2.75	Overmature
	GML-63	553	0.02	0.08	5.82	2.80	Overmature
	JZC-41	532	0.08	0.52	6.14	3.23	Overmature
	TMC-27	536	0.04	1.1	7.20	3.00	Overmature
	LMQ-08	563	0.03	0.68	5.34	3.12	Overmature

Table 2. *Cont.*

	WBD-01	586	0.05	0.09	6.72	2.86	Overmature
	WBD-05	595	0.03	0.11	4.20	2.99	Overmature
	MT-YP-09	585	0.02	0.09	9.47	2.16	Overmature
	MT-YP-11	582	0.02	0.15	10.79	2.08	Overmature
Longtan Formation	MT-YP-19	587	0.01	0.03	3.90	2.19	Overmature
	MT-YP-21	593	0.02	0.13	7.10	2.55	Overmature
	MT-YP-25	589	0.01	0.06	5.00	2.36	Overmature
	MT-YP-35	528	0.12	5.97	10.14	2.08	Overmature
	MT-YP-38	591	0.01	0.36	7.88	2.23	Overmature
	MT-YP-40	595	<0.01	0.01	1.22	2.37	Overmature

3.2.3. Maturity

In order to become a potential shale gas exploration target, the maturity of shale must enter the gas-producing window [30,31]. $R_{o,max}$ of shale samples indicate that the shale collected from Ceshui and Longtan formations has entered the large-scale gas production stage. The $R_{o,max}$ value of shale from the Ceshui Formation is between 2.37 and 3.51%, with an average of 2.95%. The $R_{o,max}$ value of all samples is greater than 2%. It indicates that the samples of the Ceshui Formation are all in the overmature stage. The sample $R_{o,max}$ of the Longtan Formation was lower than that of the Ceshui Formation, ranging from 1.34 to 2.99%, with an average of 2.16%. Most of the samples' $R_{o,max}$ is above 2%, indicating that most of the samples are in the over-mature stage.

In short, the shale of the Chenlei Sag's hydrometric and Longtan Formation has a high organic matter abundance, and its types are humic, such as II$_2$ and III types. The overall maturity is high and has exceeded the high-mature to over-mature stage. It has begun to generate large-scale gas and has a certain thickness. It is a favorable source rock for large-scale shale gas generation in the study area.

3.3. Shale Reservoir Characteristics

3.3.1. Mineral Composition Characteristics

Shale gas is generally adsorbed on the surface of organic matter, kerogen, and clay minerals, or is free in micropores and microfractures. The mineral composition is the basis for an in-depth study of the adsorption capacity and matrix porosity of shale reservoirs [32]. The mineral components of shale mainly include brittle minerals (quartz, calcite, feldspar, etc.) and clay minerals such as illite, kaolinite, chlorite, and illite mixed layers. Brittle minerals mainly control the development of fractures and affect the reservoir space and permeability of the reservoir, which in turn determines the effect of reservoir fracturing. A certain amount of clay minerals can adsorb gas [33,34]. Therefore, the key to shale gas research is to find mud shale with high organic matter content, high brittle mineral content, moderate clay mineral content, and crack development that is easy to artificial fracturing.

The whole rock mineral composition of the Ceshui Formation in Chenlei Depression is mainly quartz and clay minerals; some samples are rich in calcite, and the content of feldspar is low. The brittle mineral content is 30–80% and the clay mineral content is 10–40% (Figure 7). The whole rock mineral composition of the Longtan Formation is mainly quartz and clay minerals (Figure 8). Some samples are rich in calcite; the content of brittle minerals is 20–60%; and the content of clay minerals is 20–70%, which is not conducive to the formation of fractures but is conducive to the adsorption of shale gas. The content of brittle minerals in the shale of the Ceshui and Longtan formations in the Chenlei Depression is more than 40%, which is conducive to artificial fracturing in the later stage. Appropriate clay minerals are beneficial to gas adsorption.
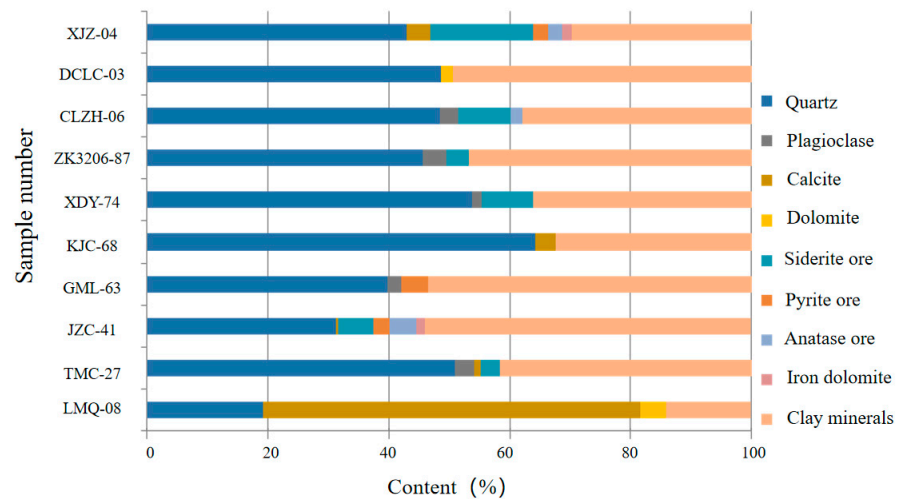
Figure 7. Bar chart of X-ray diffraction (whole rock) test results of organic-rich shale of Ceshui Formation in the study area.
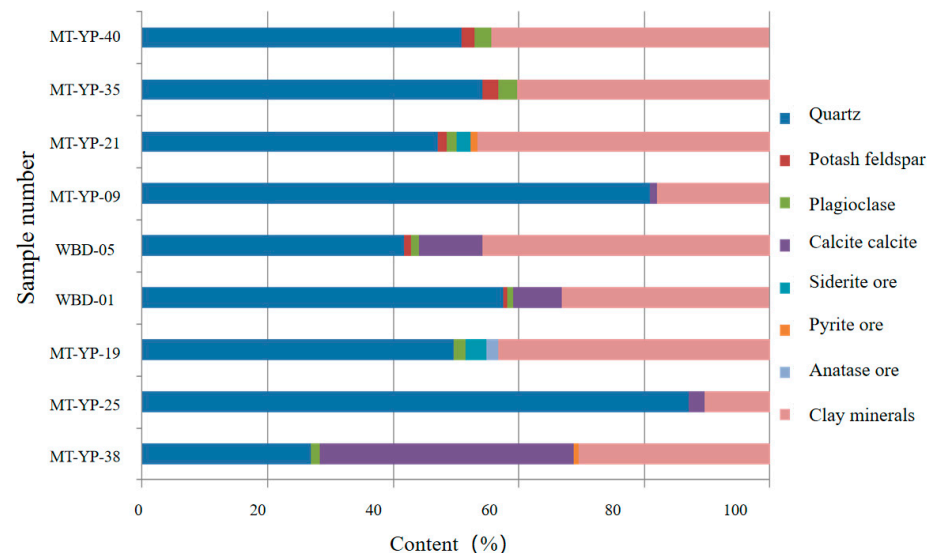

Figure 8. Bar chart of X-ray diffraction (whole rock) test results of organic-rich shale of Longtan Formation in Chenlei Sag.

3.3.2. Porosity and Permeability Characteristics

Shale reservoirs have typical characteristics of low porosity and low permeability [35], with porosity often less than 10% and permeability generally less than 1×10^{-3} μm^2. Physical property analysis of shale samples from the Ceshui and Longtan formations in the Chenlei Sag shows that the porosity and permeability of the shale from the Ceshui and Longtan formations are generally low (Figure 9), among which the porosity of the shale from the Ceshui Formation is 0.5~5.4%, with an average of 2.8%. Samples with porosity less than 3% account for more than 65% of the total samples. The permeability is 0.0002~1×10^{-3} μm^2, with an average of 0.013×10^{-3} μm^2, and more than 50%. The sample permeability is lower than 0.01×10^{-3} μm^2. The Longtan Formation mud shale has good porosity and permeability characteristics, with a porosity between 1.1% and 4.8%, with an average of 26%, and a permeability of 0.004–0.46×10^{-3} μm^2, with an average of 0.045×10^{-3} μm^2. In contrast, the porosity of major gas-producing shale reservoirs in the United States is concentrated at 4.22% to 6.51%, and the permeability is generally lower than 0.1×10^{-3} μm^2 [36]. The porosity of the mud shale in the Chenlei Sag is slightly lower than that in the Longtan Formation, and the permeability is not much different, indicating that the mud shale reservoir characteristics in the study area are better.
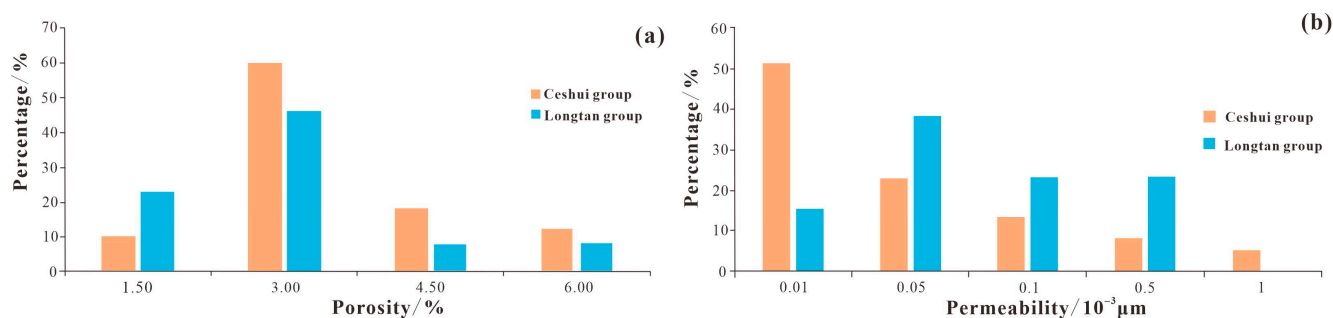
Figure 9. Distribution of porosity and permeability of Ceshui and Longtan formations in Chenlei Sag. ((**a**) Porosity Characteristics; (**b**) Permeability Characteristics).

The low-temperature nitrogen adsorption experimental data also show (Table 3) that the overall pore structure of the shale in the Chenlei Sag's Ceshui and Longtan formations is better, and its specific surface area and total pore volume are both higher (the average specific surface area is 12.21 m^2/g, respectively) and 8.36 m^2/g. The total pore volumes are 24.87×10^{-3} cm^3/g and 14.32×10^{-3} cm^3/g, respectively, and the most probable pore diameters are larger (7.05 and 4.07 nm, respectively), which is beneficial to the development of shale gas. It has good adsorption and storage potential.

Table 3. Statistics of experimental data of low-temperature nitrogen adsorption of shale samples.

Sampling Layer	Sampling No.	Specific Surface Area/m^2/g	The Most Probable Aperture/nm	Total Pore Volume/10^{-3} cm^3/g
Ceshui Formation	CLZH-06	12.61	4.05	20.49
	DCLC-03	11.38	4.07	16.33
	XJZ-04	12.84	4.04	20.64
	ZK3206-87	15.64	18.80	39.12
	XDY-74	10.81	18.79	47.21
	KJC-68	12.59	18.88	27.54
	GML-63	12.79	5.87	18.63
	JZC-41	12.88	5.37	20.04
	TMC-27	13.97	3.71	13.52
	LMQ-08	12.87	4.84	16.85
Longtan Formation	WBD-01	16.698	4.042	26.07
	WBD-05	13.073	4.065	19.65
	MT-YP-09	6.987	4.066	14.87
	MT-YP-11	7.602	4.3	11.53
	MT-YP-19	2.83	4.03	5.947
	MT-YP-21	7.668	4.068	16.23
	MT-YP-25	7.017	4.048	16.4
	MT-YP-35	8.489	4.037	11.58
	MT-YP-38	5.368	4.059	11.34
	MT-YP-40	7.533	4.063	18.41

3.3.3. Pore and Crack Characteristics

The development of shale pores and fractures in the reservoir directly affects the storage performance of the reservoir and has a great impact on the accumulation, later

preservation, and reservoir modification of shale gas [37]. This paper divides the pores in the Chenlei Sag Ceshui and Longtan formations into inorganic pores, organic pores, and micro-cracks based on their development locations and pore origins. Inorganic pores are further divided into intergranular pores, intercrystalline pores, and intragranular pores.

Intergranular pores in shale are developed at the contact point of mineral particles, which are mainly lamellar clay minerals (Figure 10a,b). They are characterized by concentrated development, complex cementation, poor sorting, and diverse pore shapes, with polygonal shapes and elongated strip shapes being the main ones. In the shale samples, the pyrite intergranular pores are well developed (Figure 10c), and the pyrite is mostly in the form of a regular cube or pentagonal dodecahedron. Organic matter and partial symbiosis. The integrate pores developed in the particles, and the integrate pores developed well in the clay mineral layer, mainly the Imon mixed layer. (Figure 10d). The pores formed by other minerals are few, and the dissolution pores of carbonate minerals can be seen under the microscope (Figure 10e).
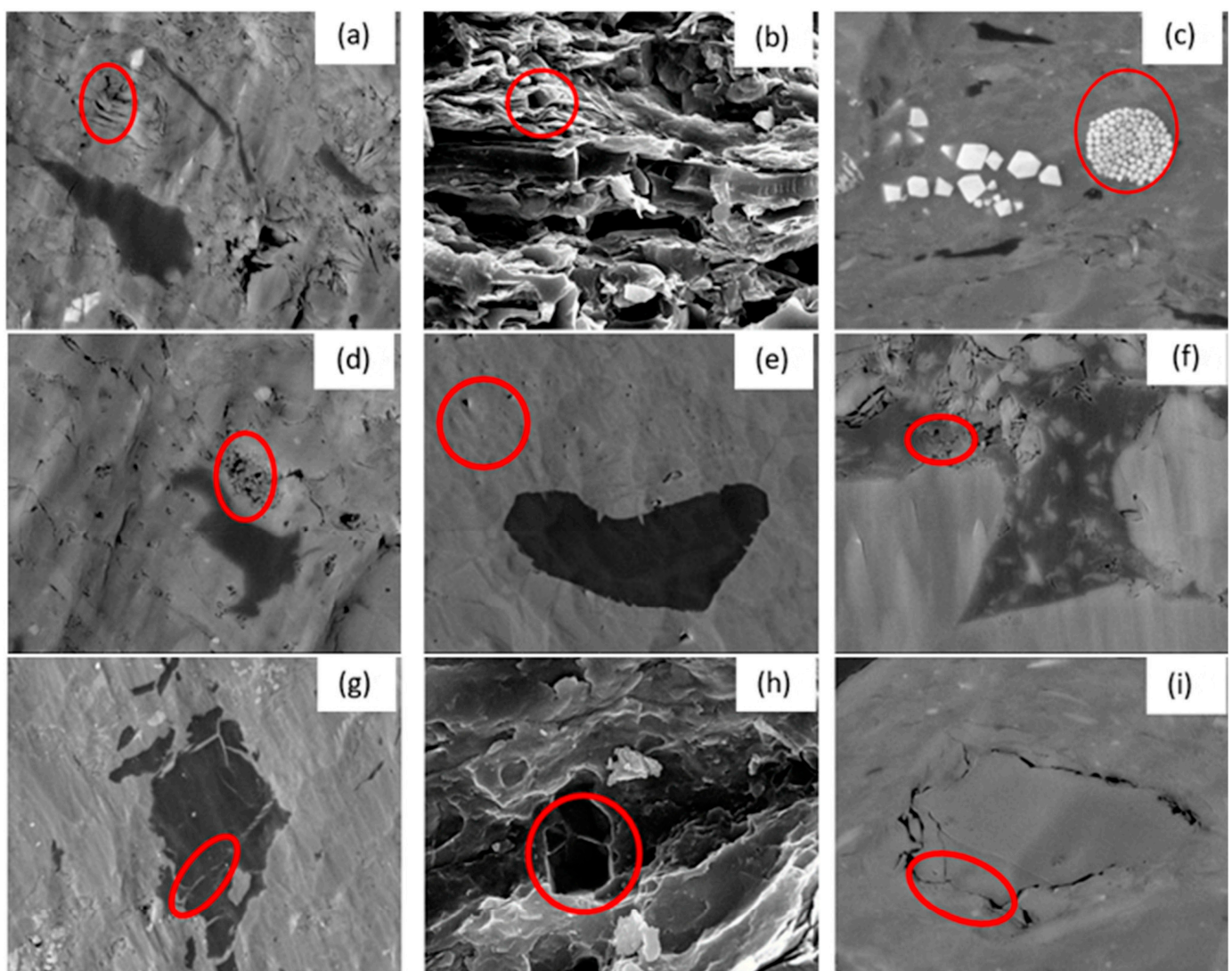
Figure 10. Pore morphology and characteristics of shales from the Ceshui and Longtan formations in Chenlei Sag. ((**a**) Flaky clay mineral interstices; (**b**) illite intergranular pores; (**c**) strawberry pyrite, intergranular pores; (**d**) mineral dissolution pores; (**e**) carbonate mineral dissolution pores; (**f**) organic matter pores; (**g**) organic matter micro-cracks are filled; (**h**) asphaltene body mold pores; (**i**) Micro-cracks).

Organic matter pores are ubiquitous in shale [38], with pore sizes ranging from a few nanometers to hundreds of nanometers. The connectivity between pores is excellent, and most organic matter pores are distributed in circular or elliptical shapes (Figure 10f). In some samples, an organic matter particle with a diameter of several microns can contain many nanopores, but some organic matter does not develop pores. Asphaltene mold pores formed by mineral exfoliation were found in some samples (Figure 10h).

Microfractures play an important role in the seepage of shale gas and are the bridge connecting microscopic pores and macroscopic fractures, which are generally micron-scale [39]. Experiments have found that both organic matter particles and clay minerals can develop micro-cracks. Micro-cracks developed inside organic matter are generally straight, small, and do not extend long. Some organic matter micro-cracks are filled with minerals (Figure 10g). The shapes of micro-cracks between minerals are diverse (Figure 10i). Some of them may be formed due to dehydration and shrinkage of the mineral matrix. They are densely developed, mostly obtuse triangle shapes, with large pore sizes and good connectivity.

3.4. Gas-Bearing Characteristics of Shale

Gas-bearing property is an important criterion for evaluating shale gas resource potential and whether it has development value [40]. The desorption method was used to perform on-site analysis on the shale cores of the Ceshui and Longtan formations obtained from four drilling wells in the study area. The results showed that the gas content of the shale in the Ceshui Formation varied from 0.31 to 2.6 cm^3/g, with an average of 1.6 cm^3/g. The gas content of the Longtan Formation shale varies from 0.42 to 5 cm^3/g, with an average of 2.1 cm^3/g. The overall gas content is high, confirming that the shale gas of the Ceshui and Longtan formations in the study area has good resource potential. The isothermal adsorption experiment shows that the maximum adsorption volume of the shale Ceshui Formation is balanced at 1~2 MPa, and the maximum adsorption capacity is between 1.2~6 cm^3/g, showing good adsorption capacity (Figure 11a,b). The Longtan Formation of shale samples maximum adsorption volume in the balance of 1.5 MPa, adsorption capacity of 0.5~5.2 cm^3/g (Figure 11c,d). The shale of the Ceshui and Longtan formations is the lowest industrial standard at 1 cm^3/g under pressure less than 2 MPa, showing good mining potential.
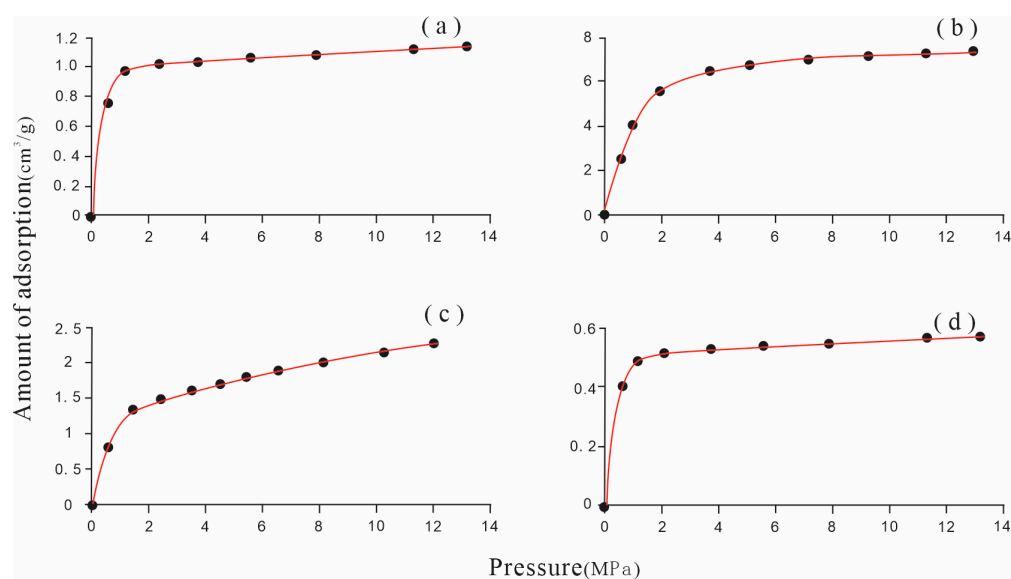

Figure 11. Typical isotherm adsorption curve of shales in Cehui and Longtan formations of Chenlei Sag. ((**a**) the shale Ceshui Formation a; (**b**) the shale Ceshui Formation b; (**c**) the Longtan Formation of shale sample c; (**d**) the Longtan Formation of shale sample d).

Based on the isothermal adsorption results and analytical gas content results, there are good shale gas displays in the study area, which has the potential to form a good shale gas reservoir.

4. Conclusions

In this paper, we discuss total organic carbon determination (TOC), kerogen microscopic component identification, mineral X-ray diffraction, scanning electron microscopy, and low-temperature nitrogen adsorption experiments. The geological conditions for the formation of shale gas reservoirs in the coal bearing strata of Chenlei Depression, Hunan Province, have been studied in detail. Moreover, the main shale gas-bearing strata and their physical characteristics in the coal bearing strata of Chenlei Depression, Hunan Province, have been studied. On this basis, the gas content of shale in the water and Longtan formations has been determined by using high-temperature and high-pressure isothermal adsorption tests. The results are as follows:

(1) The shale thickness of the water measuring group is lower, with an average thickness of about 30 m. The thickness is highest in the southern part of the depression center (nearly 70 m), then decreases towards the north. In the Leiyang and Chenzhou areas, the shale thickness of the Longtan Formation is the highest (up to 200 m), decreasing towards the northwest and southeast edges of the depression with a thickness from 0–50 m.

(2) The TOC values of the water measurement group and the Longtan group are higher, both greater than 1%, while the other layers are below 0.4%. The organic matter types are type III and II_2, and kerogen in a small amount of samples belongs to type II_1. The maturity of shale is higher, and it has entered the stage of large-scale gas generation. The Ro of the sample collected from the water measurement group is 2.37–3.51%, with an average of 2.95%.

(3) The mineral composition of the water measurement group is composed of quartz and clay minerals, with some samples rich in calcite and a low content of feldspar. The content of brittle minerals is higher, distributed in 30~80%, while the content of clay minerals is moderate, mostly distributed at 10~40%. The mineral composition of the Longtan Formation is composed of quartz and clay minerals.

(4) The overall pore structure of the water measurement group and Longtan group shale is good, with a higher specific surface area and total pore volume (average specific surface area is 12.21 and 8.36 m^2/g, respectively), which is conducive to the occurrence of shale gas and has good adsorption and storage potential. The gas content of the water measurement group varies from 0.31 to 2.6 cm^3/g, with an average of 1.6 cm^3/g; the gas content of the Longtan Formation varies from 0.42 to 5 cm^3/g, with an average of 2.1 cm^3/g. It indicates that the water measurement group and the Longtan Formation shale gas in the study area have good resource potential.

Author Contributions: Methodology, F.L.; Software, K.W.; Formal analysis, Z.L. and J.D.; Resources, S.G.; Data curation, N.C.; Writing—review & editing, J.B.; Supervision, J.Z. (Junjian Zhang); Project administration, J.Z. (Jian Zhan). All authors have read and agreed to the published version of the manuscript.

Data Availability Statement: Data are contained within the article.

Conflicts of Interest: The authors declare no conflict of interest.

References

1. Chandra, D.; Bakshi, T.; Bahadur, J.; Hazra, B.; Vishal, V.; Kumar, S.; Sen, D.; Singh, T.N. Pore morphology in thermally-treated shales and its implication on CO_2 storage applications: A gas sorption, SEM, and small-angle scattering study. *Fuel* **2023**, *331*, 125877. [CrossRef]
2. Luo, X.; Li, Y.; Wu, C. Characteristics of mud shale reservoirs in Upper Permian Longtan Formation of Southeast Hunan depression, China. *J. Chengdu Univ. Technol. (Sci. Technol. Ed.)* **2013**, *40*, 588–594.

3. Wang, E.; Guo, T.; Li, M.; Li, C.; Dong, X.; Zhang, N.; Feng, Y. Exploration potential of different lithofacies of deep marine shale gas systems: Insight into organic matter accumulation and pore formation mechanisms. *J. Nat. Gas Sci. Eng.* **2022**, *102*, 104563. [CrossRef]
4. Li, J.; Li, H.; Yang, C.; Wu, Y.; Gao, Z.; Jiang, S. Geological Characteristics and Controlling Factors of Deep Shale Gas Enrichment of the Wufeng-Longmaxi Formation in the Southern Sichuan Basin, China. *Lithosphere* **2022**, *2022*, 4737801. [CrossRef]
5. Zhang, J.; Wang, H.; Vandeginste, V.; Miao, H.; Guo, Y.; Ji, Y.; Liu, P.; Peng, Y. Effect of litho-facies on nano-pore structure of continental shale in shuinan formation of Jiaolai Basin. *Geoenergy Sci. Eng.* **2023**, *228*, 212020. [CrossRef]
6. Tang, Q.; Zhou, L.; Chen, L.; Tan, X.; Wang, G. Development Characteristics of Shale Lithofacies in the Longmaxi Formation and their Main Controlling Factors in the Changning Area, South Sichuan Basin, SW China. *Front. Earth Sci.* **2021**, *9*, 775657. [CrossRef]
7. Li, J.; Li, H.; Yang, C.; Ren, X.; Li, Y. Geological Characteristics of Deep Shale Gas and Their Effects on Shale Fracability in the Wufeng-Longmaxi Formations of the Southern Sichuan Basin, China. *Lithosphere* **2023**, *2023*, 4936993. [CrossRef]
8. Fang, R.; Jiang, Y.; Sun, S.; Luo, Y.; Qi, L.; Dong, D.; Lai, Q.; Luo, Y.; Jiang, Z. Controlling factors of organic matter accumulation and lacustrine shale distribution in Lianggaoshan Formation, Sichuan Basin, SW China. *Front. Earth Sci.* **2023**, *11*, 1218215. [CrossRef]
9. Zhang, P.; Lu, S.; Li, J.; Wang, J.; Zhang, J.; Chen, G.; Huang, H.; Zhi, Q.; Yin, Y. Microscopic characteristics of pore-fracture system in lacustrine shale from Dongying Sag, Bohai Bay Basin, China: Evidence from scanning electron microscopy. *Mar. Pet. Geol.* **2023**, *150*, 106156. [CrossRef]
10. Wang, E.; Li, Y.; Guo, T.; Xiong, L.; Dong, X.; Wang, T.; Shi, K. Geological Features, Paleosedimentary Environment, and Organic Matter Accumulation Mechanisms of the Lacustrine Shale Oil System: A Case Study of the Jurassic Dongyuemiao Member in the Sichuan Basin. *Processes* **2023**, *11*, 2638. [CrossRef]
11. Xu, H.; Madina, M.; Yu, S.; Wang, Z.; Cheng, H.; Jiang, T. Geological Characteristics of Shale Reservoir of Pingdiquan Formation in Huoshaoshan Area, Junggar Basin. *Processes* **2023**, *11*, 2126. [CrossRef]
12. Cai, Z.; Huang, Q.; Xia, B.; Xiang, J. Differences in shale gas exploration prospects of the upper Yangtze Platform and the lower Yangtze Platform: Insights from computer modelling of tectonic development. *J. Nat. Gas Sci. Eng.* **2016**, *36*, 3642–3653. [CrossRef]
13. Shi, W.; Wang, X.; Wang, Z.; Shi, Y.; Feng, A.; Chen, N. A study on the relationship between graptolites and shale gas enrichment in the Wufeng–Longmaxi Formations of the Middle–Upper Yangtze region in China. *Arab. J. Geosci.* **2020**, *13*, 205–217. [CrossRef]
14. Zhao, L.; Li, Y.; Zou, C.; Zhao, S.; Wu, C. Palaeoweathering Conditions, Provenance, and Tectonic Setting of the Early Silurian Longmaxi Formation in the Upper Yangtze Region (Southern China): Evidence from Geochemistry. *Minerals* **2023**, *13*, 576. [CrossRef]
15. Wang, T.; Xu, Z.; Yuan, K.; Wang, X.; Ge, M. Paleoenvironment and shale gas potential of the Carboniferous Dawuba and the Cambrian Niutitang shales in the Upper Yangtze Platform, South China. *Front. Earth Sci.* **2024**, *12*, 1404178. [CrossRef]
16. Liu, W.; Gao, P.; Xiao, X.; Zhao, Y.; Xing, Y.; Li, J. Variable depositional environments and organic matter enrichment of Early Cambrian shales in the Middle Yangtze region, South China. *J. Asian Earth Sci.* **2024**, *259*, 105874. [CrossRef]
17. Qian, J.; Ma, R.; Bu, S.; Xu, F. Lithofacies-paleogeographical characteristics of marine shale series of strata in Xiangzhong and Xiangdongnan depressions, Hunan, China. *J. Chengdu Univ. Technol. (Sci. Technol. Ed.)* **2013**, *40*, 688–695.
18. Lin, D.; Xi, Z.; Tang, S.; Lash, G.G.; Guo, Q.; Wang, H.; Zhu, Y. Organic matter enrichment in shale deposited proximal to paleo-uplifts and its impact on shale gas exploration.Palaeogeography, Palaeoclimatology. *Palaeoecology* **2024**, *633*, 111900. [CrossRef]
19. Zhang, B.; Yao, S.; Hu, W.; Wu, Y.; Yu, W.; Yu, H. Hydrocarbon source rock characteristics and shale gas potential of Permian marine shales in the Lower Yangtze region of South China. *AAPG Bull.* **2024**, *108*, 719–749. [CrossRef]
20. Taotao, C.; Mo, D.; Hu, L.; Yanran, H.; Hurssthouse, S. Shale gas potential of Yanguanjie Formation and Longtan Formation in central and southeastern Hunan Province. *Coal Geol. Explor.* **2019**, *47*, 94–103.
21. Yin, S.; Xiao, J. Relationship between Geological Structure Characteristics and Coal Seams in Chenlei and Lianshao Coal-bearing Areas. *West-China Explor. Eng.* **2014**, *26*, 138–141.
22. Shi, W.; Li, Q.; Li, J. Structural evolution and hydrocarbon accumulation in Southeast Hunan Depression. *Land Resour. Her.* **2006**, *S1* (Suppl. S1), 15–21.
23. Xu, G.S.; Zhang, Z.; Luo, X.P.; Zhang, W.; Bu, S.F. Gas-bearing characteristics and affected factors of Upper Paleozoic shale in depressions of Central Hunan and Southeast Hunan, China. *J. Chengdu Univ. Technol. (Sci. Technol. Ed.)* **2013**, *40*, 577–587.
24. Ahmadi, Y.; Mansouri, M.; Jafarbeigi, E. Improving Simultaneous Water Alternative Associate Gas Tests in the Presence of Newly Synthesized γ-Al2O3/ZnO/Urea Nano-Composites: An Experimental Core Flooding Tests. *ACS Omega* **2023**, *8*, 1443–1452. [CrossRef]
25. Zhang, P.F.; Wu, H.; Lu, S.F.; Wang, J.J.; Li, W.B.; Yin, Y.J.; Zhou, N.W.; Zhang, J.J.; Chen, G.H.; Yi, Y.J.; et al. The occurrence of pore fluid in shale-oil reservoirs using nuclear magnetic resonance: The Paleogene Funing Formation, Subei Basin, Eastern China. *Mar. Pet. Geol.* **2024**, *167*, 106986. [CrossRef]
26. Xu, J.; Guo, W.; Yang, B.; Ma, D.; Zhao, L.; Liu, H.; Ji, H.; Tao, H. Nanopore Characteristics of the Cambrian Niutitang Formation Organic-Rich Shales in the Middle Yangtze Region and Its Formation Controlling Factors. *Geofluids* **2023**, *2023*, 2070913. [CrossRef]
27. Hu, L.; Xue, X.; Zhang, Y.; Ma, Y.; Yunnan CBM Resources Exploration and Development Co., Ltd. Accumulation Conditions Analysis of Shale Gas of Upper Permian Longtan Formation of Xuanwei Area in Eastern Yunnan. *Unconv. Oil Gas* **2018**, *5*, 29–33.

28. Wang, Z.; Xiao, Z.; Yang, R.; Huang, Y. A Study on Carboniferous Ceshui Formation Shale Gas Generation Material Basis in Central Hunan. *Coal Geol. China* **2013**, *25*, 19–21+31.

29. Zhou, N.; Lu, S.; Zhang, P.; Wang, M.; Xiao, D.; Li, J.; Chen, G.; Wang, J.; Zhang, Y.; Lin, Z. Continental shale gas dynamic enrichment and evolution over geological time. *Int. J. Coal Geol.* **2021**, *251*, 103914. [CrossRef]

30. Zhang, P.; Lu, S.; Wang, J.; Li, W.; Yin, Y.; Chen, G.; Zhou, N.; Wu, H. Microscopic occurrence and distribution of oil and water in situ shale: Evidence from nuclear magnetic resonance. *Petrol. Sci.* **2024**, 1995–8226. [CrossRef]

31. Zhang, H.; Wang, X.; Jia, C.; Li, J.; Meng, Q.; Jiang, L.; Wang, Y.; Bai, X.; Zheng, Q. Whole petroleum system and hydrocarbon accumulation model in shallow and medium strata in northern Songliao Basin, NE China. *Pet. Explor. Dev. Online* **2023**, *50*, 784–797. [CrossRef]

32. Qi, P.; Xue, P.; Zhao, Q. Research on evaluation methods and characteristics of shale gas reservoirs in Shanxi formation in Xiasiwan area, Ordos basin. *Unconv. Oil Gas* **2019**, *6*, 10–17.

33. Zou, C.; Dong, D.; Wang, S.; Li, J.; Li, X.; Wang, Y.; Li, D.; Cheng, K. Geological characteristics, formation mechanism, and resource potential of shale gas in China. *Pet. Explor. Dev.* **2010**, *37*, 641–653. [CrossRef]

34. Ma, B.; Hu, Q.; Yang, S.; Zhang, T.; Qiao, H.; Meng, M.; Zhu, X.; Sun, X. Pore structure typing and fractal characteristics of lacustrine shale from Kongdian Formation in East China. *J. Nat. Gas Sci. Eng.* **2021**, *85*, 103709. [CrossRef]

35. Lan, B.; Zhao, F.; Li, S.; Jiang, H.; Liu, S.; Zhang, Z. Investigation of the Enrichment and Accumulation of Normal Pressure Shale Gas in Anchang Syncline Outside of Sichuan Basin. *Front. Earth Sci.* **2022**, *9*, 802142. [CrossRef]

36. Dong, C.Y.; Xie, Z.Y.; Zhu, H.; Guo, J.Y.; Zhang, L.; Dai, X.; Yang, C.L. New Insight for Gas Source and Gas Accumulation Modes of Middle Permian in Central Sichuan Basin. *J. Xi'an Shiyou Univ. (Nat. Sci.)* **2017**, *32*, 18–23, 31.

37. Wu, C. Study on fractal features of shale pore based on low-temperature nitrogen absorption experiment. *Unconv. Oil Gas* **2018**, *5*, 14–20.

38. Zhang, T.; Zhang, X. Comparative study on qualitative and quantitative methods for shale pore characterization. *Nat. Gas Explor. Dev.* **2017**, *40*, 34–43.

39. Xiao, D.; Lu, S.; Fang, D. Pore connectivity of marine high-maturity shale gas reservoirs: A case study in Longmaxi formation, Pengshui area. *Reserv. Eval. Dev.* **2019**, *9*, 45–53.

40. Long, P.Y.; Zhang, J.C.; Tang, X.; Nie, H.K.; Liu, Z.J.; Han, S.B.; Zhu, L.L. Feature of Muddy Shale Fissure and Its Effect on Shale Gas Exploration and Development. *Nat. Gas Geosci.* **2011**, *22*, 525–532.